Electronic structure of Ag-induced $\sqrt{3}\times\sqrt{3}$ and $\sqrt{21}\times\sqrt{21}$ superstructures on the Si(111) surface studied by angle-resolved photoemission spectroscopy and scanning tunneling microscopy

Xiao Tong,[1,*] Satoru Ohuchi,[2] Norio Sato,[2] Takehiro Tanikawa,[2] Tadaaki Nagao,[2,3] Iwao Matsuda,[4] Yoshinobu Aoyagi,[1] and Shuji Hasegawa[2,3]

[1]*The Institute of Physical and Chemical Research (RIKEN), 2-1 Hirosawa, Wako, Saitama, 351-0198, Japan*

[2]*Department of Physics, University of Tokyo, 7-3-1 Hongo, Bunkyo-ku, Tokyo 113-0033, Japan*

[3]*Core Research for Evolutional Science and Technology, The Japan Science and Technology Corporation, Kawaguchi Center Building, Hon-cho 4-1-8, Kawaguchi, Saitama 332-0012, Japan*

[4]*Department of Chemistry, University of Tokyo, 7-3-1 Hongo, Bunkyo-ku, Tokyo 113-0033, Japan*

(Received 23 July 2001; published 6 November 2001)

Polarization-dependent angle-resolved photoemission spectroscopy was used to analyze the electronic band structure of the Si(111)-$\sqrt{21}\times\sqrt{21}(R\pm10.89°)$-Ag surface induced by adding submonolayer Ag atoms on top of the Si(111)-$\sqrt{3}\times\sqrt{3}$-Ag surface at 140 K, together with a refinement of the electronic states of the initial $\sqrt{3}\times\sqrt{3}$-Ag substrate itself. The surface-state band crossing the Fermi level on the the $\sqrt{3}\times\sqrt{3}$-Ag surface was found to have similar dispersions in both $\bar{\Gamma}$-$\bar{K}$ and $\bar{\Gamma}$-$\bar{M}$ directions around the $\bar{\Gamma}$ point of the $\sqrt{3}\times\sqrt{3}$ surface Brillouin zone, and consist mainly of components parallel to the surface with no measurable polarization dependence. The five intrinsic surface-state bands observed on the $\sqrt{3}\times\sqrt{3}$-Ag surface basically remained in the $\sqrt{21}\times\sqrt{21}$-Ag structure, but shifted down in energy position from the Fermi level by about 0.4 eV. This is due to electron transfer from the Ag adatoms to the substrate, suggesting that the Ag adatoms in the $\sqrt{21}\times\sqrt{21}$-Ag phase sit on a nearly unaltered $\sqrt{3}\times\sqrt{3}$-Ag substrate, and do not make any orbital hybridization with the substrate. Only one parabolic band crossing the Fermi level was found on the $\sqrt{21}\times\sqrt{21}$-Ag surface, for which distribution in real space is observed by bias-dependent scanning tunneling microscopy. This result is in contrast to two metallic bands on the $\sqrt{21}\times\sqrt{21}$ phase induced by Au or Cu adatoms on the $\sqrt{3}\times\sqrt{3}$-Ag substrate reported in previous papers.

DOI: 10.1103/PhysRevB.64.205316 PACS number(s): 73.20.At, 73.25.+i, 68.35.−p

I. INTRODUCTION

$\sqrt{21}\times\sqrt{21}$ surface superstructures are known to be induced by submonolayer (around 0.2 ML) adsorption of noble- or alkali-metal atoms on top of the Si(111)-$\sqrt{3}\times\sqrt{3}$-Ag surface at room temperature (RT) or lower temperature (LT).[1–5] Although in all of the $\sqrt{21}\times\sqrt{21}$ phases the additionally deposited atoms are considered to arrange themselves periodically without breaking the $\sqrt{3}\times\sqrt{3}$-Ag underlying framework, the details of the atomic arrangements are still open questions. The atomic arrangements of the $\sqrt{21}\times\sqrt{21}$ phases are believed to be quite similar to each other.[6] An interesting point is that only monovalent metal adatoms commonly induce $\sqrt{21}\times\sqrt{21}$ structures; the divalent and trivalent adatoms cannot make any superstructures on the $\sqrt{3}\times\sqrt{3}$-Ag surface. A common property of all of $\sqrt{21}\times\sqrt{21}$ surfaces is high electrical conductances.[7,8,10,5] At the optimum coverage of adatoms for the $\sqrt{21}\times\sqrt{21}$ phases, the surface conductance showed maxima, while further deposition of the adatoms instead reduced the conductance accompanying the destruction of $\sqrt{21}\times\sqrt{21}$ structures. The surface electronic states of Au- and Cu-adatom-induced $\sqrt{21}\times\sqrt{21}$ structures at RT were already investigated by photoemission spectroscopies to clarify the origin of the high electrical conductances.[9,10] As a result, metallic surface-state bands with large dispersions were found, for which the Fermi wave numbers are much larger than that of the initial $\sqrt{3}\times\sqrt{3}$-Ag surface. This is the origin of the high conductances, rather than the surface space-charge layers.

The purpose of the present paper is to present the surface electronic structure of the Ag-adatom-induced $\sqrt{21}\times\sqrt{21}$ structure at LT (140 K), revealed by angle-resolved photoemission spectroscopy (ARPES) with synchrotron radiation, and to compare the results with the cases of Au- and Cu-induced $\sqrt{21}\times\sqrt{21}$ surfaces. Only one parabolic surface-state band crossing the Fermi level (E_F) with a large Fermi wave number was found, which should be contrasted to two metallic bands found on the Au- or Cu-induced $\sqrt{21}\times\sqrt{21}$ phase. The metallic band, rather than the surface space-charge layer, causes the high surface conductance. The real-space distribution of the surface-state band is visualized by bias-dependent scanning tunneling microscopy (STM) at LT. By comparing the surface-state bands on the initial $\sqrt{3}\times\sqrt{3}$-Ag surface that was reinvestigated here in more detail at deeper binding states at LT, the feature of the electronic states of the $\sqrt{21}\times\sqrt{21}$ phase was revealed. The surface states of the initial $\sqrt{3}\times\sqrt{3}$-Ag substrate were basically preserved in the $\sqrt{21}\times\sqrt{21}$-Ag phase, only with some shifts in the energy position. This provides a basis for the expectation that the $\sqrt{3}\times\sqrt{3}$-Ag framework is preserved in the $\sqrt{21}\times\sqrt{21}$ phase. We begin with a refinement of the electronic structure of the initial $\sqrt{3}\times\sqrt{3}$-Ag surface, because to our knowledge this is the first measurement by ARPES at LT, so that the surface-state peaks are resolved clearly and some interesting information is obtained.

II. EXPERIMENT

The experiments were performed in separate UHV chambers, one of which was an ARPES machine (VG-ADES 400)

on a vacuum-ultraviolet beam line BL-7B (Research Center for Spectrochemistry, University of Tokyo) at the Photon Factory in Tsukuba, Japan; the other was a LT-STM machine (UNISOKU-USM 501) at the Department of Physics, University of Tokyo. The substrate was an *n*-type Si(111) wafer of 20-Ω cm resistivity at RT, and its typical dimension was $25\times4\times0.4$ mm^3. A clear 7×7 LEED (low-energy electron diffraction) pattern was produced by flashing the sample at 1200 °C several times by direct current about 10 A through it in vacuum of 10^{-10} Torr range. The Si(111)-$\sqrt{3}\times\sqrt{3}$-Ag structure was made at a substrate temperature of 450 °C by depositing about 1 ML of Ag atoms, whose LEED pattern is shown in Fig. 1(a). After cooling the substrate down to 140 K, the Si(111)-$\sqrt{21}\times\sqrt{21}$-Ag structure was formed by depositing Ag atoms of about 0.14–0.19 ML coverage onto the $\sqrt{3}\times\sqrt{3}$-Ag surface at a rate of 0.50 ML/min. Its LEED pattern is shown in Fig. 1(b), which is a double-domain pattern of the $\sqrt{21}\times\sqrt{21}(R\pm10.89°)$ phase. The sharp fractional-order spots showing the $\sqrt{21}\times\sqrt{21}$ superstructure are clearly seen around the $\sqrt{3}\times\sqrt{3}$ fractional spots. The coverage of Ag was calibrated in such a way that 1 ML of Ag is needed for a complete conversion in a LEED pattern from the 7×7 to the $\sqrt{3}\times\sqrt{3}$ Ag.[14,15]

ARPES spectra of the $\sqrt{3}\times\sqrt{3}$-Ag and $\sqrt{21}\times\sqrt{21}$-Ag surfaces were measured using linearly polarized synchrotron radiation at a photon energy of 21.2 eV. The overall angular and energy resolutions were about 1.5° and 0.1 eV, respectively. In order to investigate the symmetry properties of surface wave functions along axes in a surface Brillouin zone (SBZ) containing mirror-symmetry planes, we adopted two different measurement geometries denoted as A_+ and $A_\pm$, respectively, as shown in Fig. 1(c).[11] According to the symmetry selection rule, only photoelectrons from initial states of even symmetry with respect to the [101] plane are detected in the A_+ geometry, while photoelectrons from both even- and odd-symmetry states are probed in the $A_\pm$ geometry. The ARPES spectra shown in this paper were recorded in the A_+ geometry, if not specified differently. The acquired ARPES spectra were compiled into gray-scale two-dimensional (2D) band dispersion diagrams with use of the second derivatives of the original spectra.[12,13] The brightness of the brighter features in the diagrams is roughly proportional to I/W, where I and W are the intensity and width of a peak in the spectra, respectively. In this way, one can easily see not only the dispersive behavior of peaks but also the evolutions in their intensities and widths in the $K_\parallel$ space.[12,13]

For STM observations, similar procedures were followed with help of reflection-high-energy electron diffraction instead of LEED to prepare the sample surfaces, except that additional Ag adatoms were deposited onto the $\sqrt{3}\times\sqrt{3}$-Ag surface at the cold STM stage around 70 K to obtain the $\sqrt{21}\times\sqrt{21}$-Ag structure. The temperature difference between 140 and 70 K during the preparations did not cause any essential difference in the structure of the $\sqrt{21}\times\sqrt{21}$-Ag phase. Electrochemically sharpened W tips were used following *in situ* cleaning in UHV to obtain constant-current images at around 70 K with the STM attached to a liquid nitrogen container.

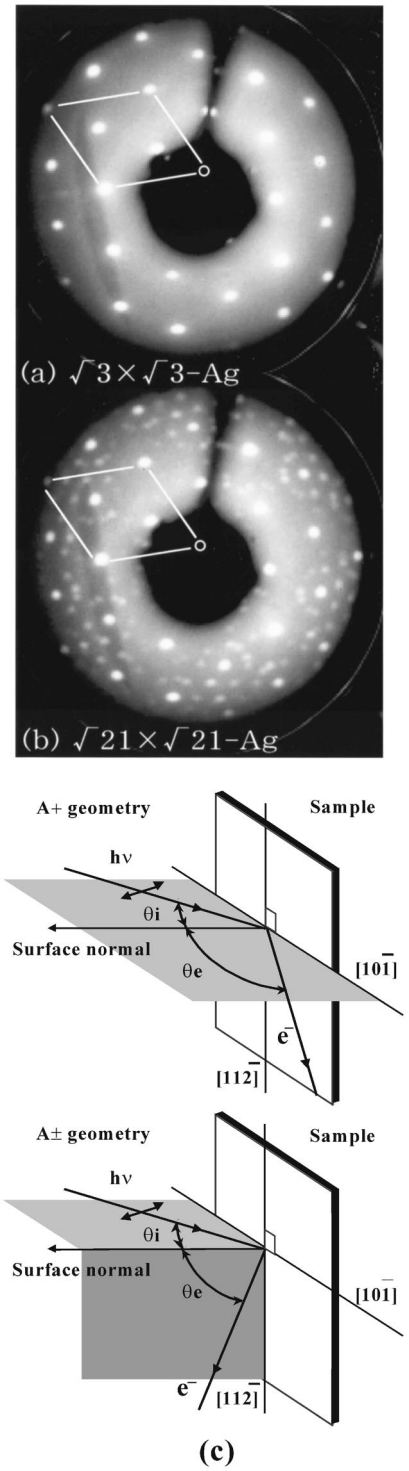

FIG. 1. LEED patterns taken at 140 K from (a) the Si(111)-$\sqrt{3}\times\sqrt{3}$-Ag surface and (b) the Si(111)-$\sqrt{21}\times\sqrt{21}$-Ag surface. The 1×1 unit cell in a reciprocal lattice is drawn. (c) Two different geometries of polarization-dependent ARPES measurements. In the A_+ geometry, the incident photon beam and its polarization are in a plane defined by the surface-normal and [101] emission directions. In the $A_\pm$ geometry, the incident photon beam and its polarization are in a plane perpendicular to the surface-normal and [112] emission directions (Ref. 11).

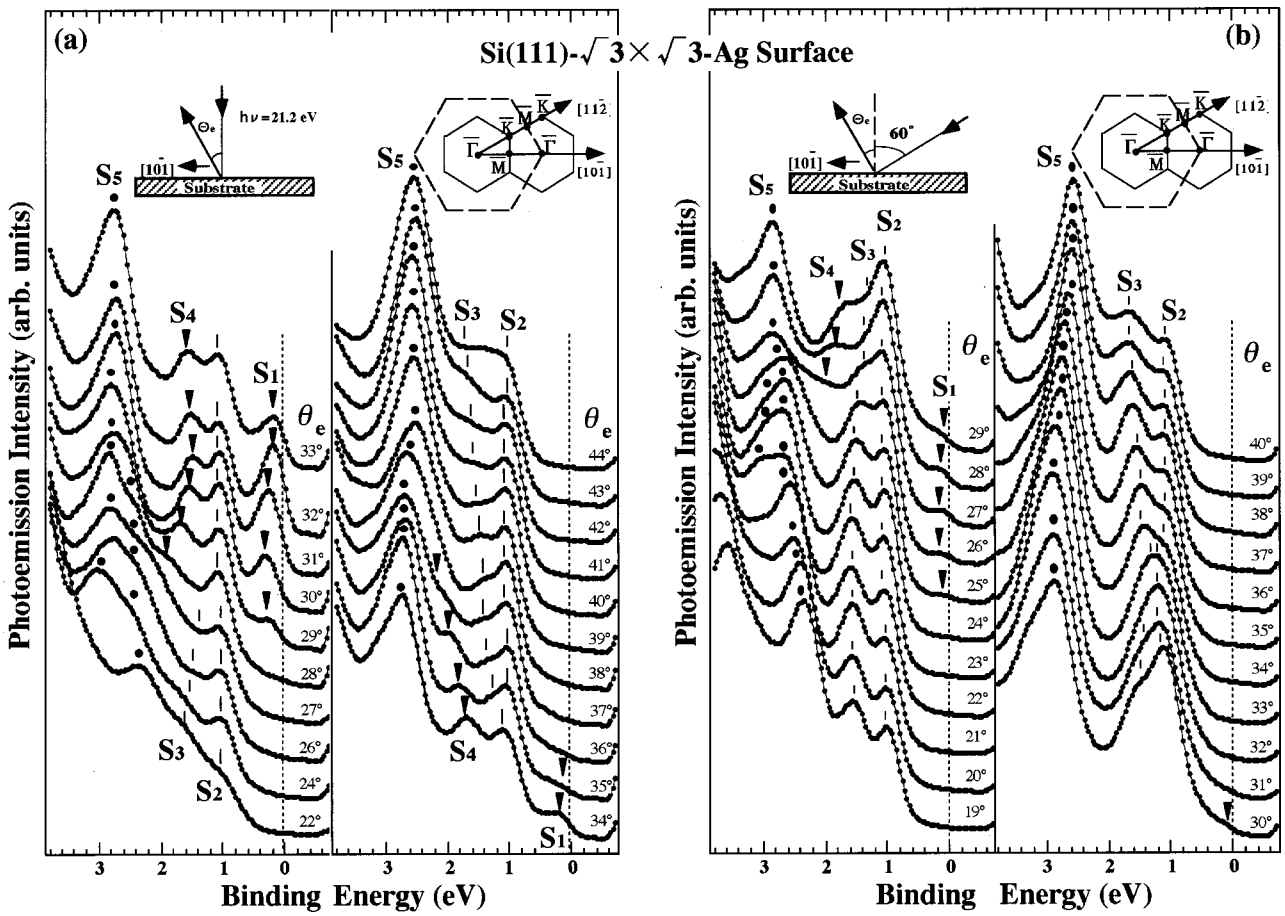

FIG. 2. ARPES spectra for the Si(111)-$\sqrt{3}\times\sqrt{3}$-Ag surface at 140 K, taken with linearly polarized synchrotron radiation of 21.2 eV, scanned along the [101] direction. The angles of incidence of photon θ_i with respect to the surface normal were (a) 0° and (b) 60°, respectively.

III. RESULTS

A. Si(111)-$\sqrt{3}\times\sqrt{3}$-Ag surface

Figures 2(a) and 2(b) show the ARPES spectra of the $\sqrt{3}\times\sqrt{3}$-Ag surface at 140 K taken along the [101] direction, with photon angles of incidence of $\theta_i=0°$ and 60° from the surface normal, respectively. The binding energy refers to E_F, that was determined from the metallic edge in an ARPES spectrum from a Ta sample holder. The corresponding gray-scale 2D band dispersion diagrams are shown in Figs. 3(a) and 3(b), respectively. The symbol Γ is the center of the second $\sqrt{3}\times\sqrt{3}$ SBZ. As shown in Fig. 2(a), a strong dispersive band near E_F is observed at emission angles around $\theta_e=29°-35°$, as indicated by arrowheads. Its bottom is located around 0.2 eV below E_F, and it disperses around the Γ point. This was called an S_1 surface-state band.[16] However, when the incident angle of photon θ_i with respect to the surface-normal is set to 60°, the intensity of the S_1 band is significantly diminished, as shown in Figs. 2(b) and 3(b). This indicates that the S_1 state is excited only by the component of the photoelectric vector parallel to the surface, i.e., the state consists mainly of p_x and p_y components (the xy plane is parallel to the surface). The first-principles calculation also shows that the S_1 state stems mostly from the Ag $5p$ orbital.[17]

The S_1 band was first observed by Johansson *et al.* with incident angles of photon $\theta_i=15°$ and 45° under A_- (it was defined as $A_\perp$ in Ref. 16) geometry, in which the electric vector of the photon was perpendicular to the plane defined by the surface normal and the [101] emission direction.[16] We believe that the independence of the emission intensity of the S_1 band upon the photon incident angle θ_i observed by Johansson *et al.* was not inconsistent with our results here, because that the electric vector of the photon in the A_- geometry was always parallel to the surface irrespective of the photon incident angle θ_i; thus it was able to excite the S_1 band at both $\theta_i=15°$ and 45°. On the other hand, Johansson *et al.* reported that the S_1 state was practically invisible in the geometry of A_+ (it was defined as $A_\parallel$ in Ref. 16) with an incident angle of the photon of $\theta_i=15°$ (Ref. 16); however, we detected a strong S_1 band even under an A_+ geometry with $\theta_i=0°$, as shown in Fig. 2(a). Therefore, it is certain that the S_1 state has no measurable polarization dependence, since a strong S_1 band can be detected in both of the A_- and A_+ geometries.

The other surface-state bands detected on the $\sqrt{3}\times\sqrt{3}$-Ag surface are indicated by S_2, S_3, S_4, and S_5 in Figs. 2 and 3. S_2 and S_3 are degenerate at the Γ point, which is consistent with the previous observations at RT.[16,9] The intensity of S_3

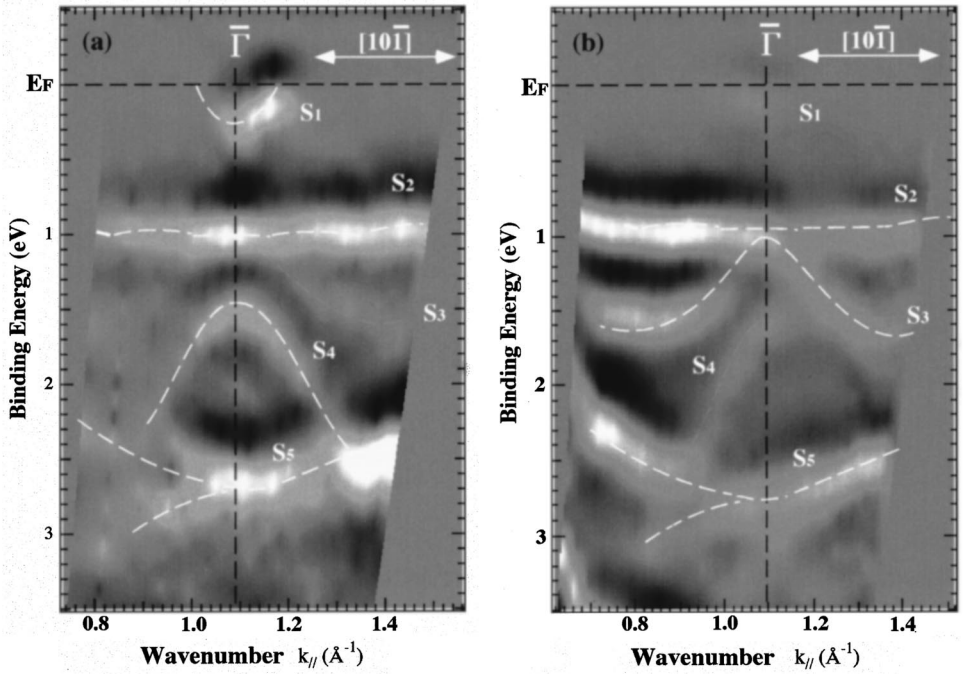

FIG. 3. Gray-scale band-dispersion diagrams for the Si(111)-$\sqrt{3}\times\sqrt{3}$-Ag surface, corresponding to the ARPES spectra in Figs. 2(a) and 2(b), respectively. The symbol $\bar{\Gamma}$ is the center in the second $\sqrt{3}\times\sqrt{3}$-surface Brillouin zone. Dashed lines are just to guide the eye, illustrating surface-state bands.

is weaker at $\theta_i=0°$, but stronger at $\theta_i=60°$. The S_4 band, with a large downward dispersion around the $\bar{\Gamma}$ point, is found here for the first time to our knowledge. Its intensity is stronger at $\theta_i=0°$, but weaker at $\theta_i=60°$. By analyzing the dependence of the intensity of each band upon the incident angle of the photon in the same way as for the S_1 band, we conclude that an S_3 state having even symmetry with respect to the mirror plane, defined by the surface-normal and [101] emission directions, consists primarily of p_z components (z is the surface-normal direction), and that S_4 is similar to S_1, stemming primarily from p_x and p_y components. The S_2 and S_5 states mainly originate from s orbitals. The theory assumes that the S_2 state consists of Ag 5s orbitals.[17] Figures 4(a) and 4(b) show the ARPES spectra and the corresponding gray-scale band dispersion diagram of the $\sqrt{3}\times\sqrt{3}$-Ag surface at 140 K along the [112] direction around the third $\sqrt{3}\times\sqrt{3}$ SBZ, respectively, under an $A_{\pm}$ condition. As shown in Fig. 4(b), an S_1 band with a large upward dispersion is detected around the $\bar{\Gamma}$ point, also in the [112] direction. We believe this is the first time an S_1 band was detected in the [112] direction; this is similar to being detected in the [101] direction although the band bottom is slightly deeper. This suggests a nearly isotropic dispersion around the $\bar{\Gamma}$ point and a circular Fermi surface, meaning a 2D nearly-free-electron-like state, as expected. The behaviors of the S_1, S_2, and S_3 states in the [112] direction are consistent with theoretical calculation by Ding *et al.*[18]

B. Si(111)-$\sqrt{21}\times\sqrt{21}$-Ag surface

Figures 5(a) and 5(b) show the angle resolved ultraviolet photoemission spectra of the $\sqrt{21}\times\sqrt{21}$-Ag surface, scanned along the [101] direction with $\theta_i=0°$ and 60°, respectively. The corresponding gray-scale band dispersion diagrams are shown in Figs. 6(a) and 6(b), respectively. The symbol $\bar{\Gamma}$ is a center in the second $\sqrt{3}\times\sqrt{3}$ SBZ. By comparing these with the spectra of the initial $\sqrt{3}\times\sqrt{3}$-Ag surface in Fig. 2, all the features of the band dispersions scarcely change in the $\sqrt{21}\times\sqrt{21}$-Ag surface even though the relative intensities among the peaks are different. A strongly dispersive peak appears near E_F, as indicated by the arrowheads at $\theta_i=29°-42°$ in Fig. 5(a), which make a parabolic band crossing E_F in Fig. 6(a). We call this the S_1^* band. It appears only near the $\bar{\Gamma}$ point of the $\sqrt{3}\times\sqrt{3}$ SBZ such as the S_1 band of the initial $\sqrt{3}\times\sqrt{3}$-Ag surface [Fig. 3(a)], but the bottom of the S_1^* band is much lower below E_F, which implies that the S_1^* band is occupied by many more electrons. However, when the angle of incidence of photon θ_i with respect to the surface normal is set to 60°, this S_1^* band is significantly diminished as shown in Figs. 5(b) and Fig. 6(b). This character is similar to the S_1 band of the initial $\sqrt{3}\times\sqrt{3}$ surface; the S_1^* state again consists mainly of p_x and p_y components. The other surface-state bands detected in the $\sqrt{21}\times\sqrt{21}$-Ag surface are indicated by D, S_2', S_3', S_4', and S_5' in Figs. 5 and 6. The bands from S_2' to S_5' have dispersions similar to the bands from S_2 to S_5 of the initial $\sqrt{3}\times\sqrt{3}$-Ag surface, but shifted toward higher binding energy by about 0.4 eV [compare Figs. 6(a) and 3(a)]. The other surface-state band denoted by D at a binding energy of about 1.0 eV with negligible dispersion is observed only on the $\sqrt{21}\times\sqrt{21}$ surface. Figure 7(a) shows a LT-STM image of the $\sqrt{21}\times\sqrt{21}$-Ag surface at 70 K. The surface is almost entirely covered by the $\sqrt{21}\times\sqrt{21}$-Ag phase. A straight boundary indicated by OPB3 running along the [112] direction is an out-of-phase-boundary of the $\sqrt{3}\times\sqrt{3}$-Ag substrate, which is decorated by some Ag adatoms, while another boundary indicated by OPB21 is an out-of-phase-boundary in the $\sqrt{21}\times\sqrt{21}$-Ag phase. The neighboring domains at OPB3 have different orientations of [112]$\pm$10.89°, as indicated by unit cells drawn

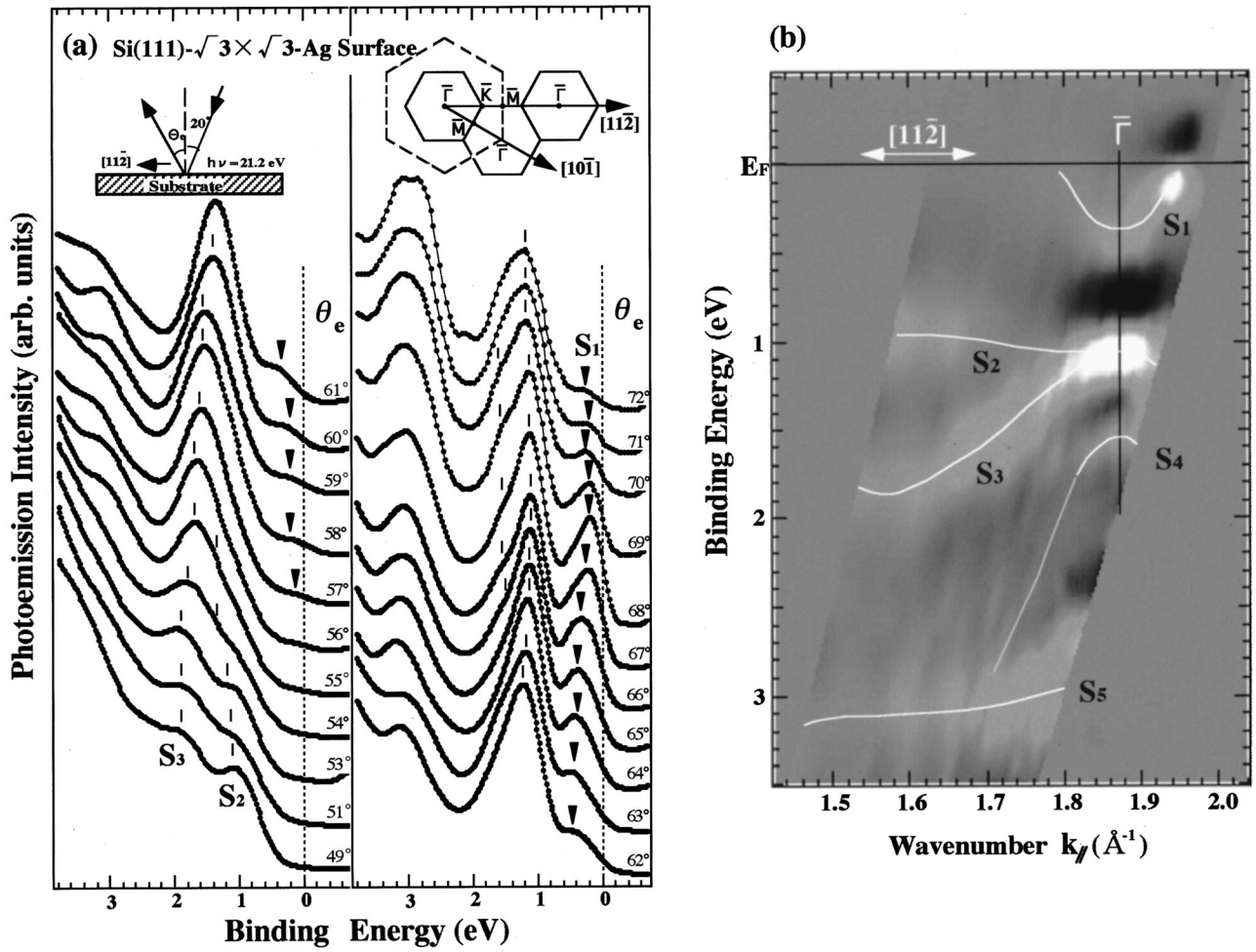

FIG. 4. (a) ARPES spectra for the Si(111)-$\sqrt{3}\times\sqrt{3}$-Ag surface at 140 K, scanned along the $[11\bar{2}]$ direction. with $\theta_i = 20°$. (b) The corresponding gray-scale band-dispersion diagram. The symbol $\bar{\Gamma}$ is the center in the third $\sqrt{3}\times\sqrt{3}$-surface Brillouin zone.

in the figure. Figure 7(b) is a magnified image of the $\sqrt{21}\times\sqrt{21}$-Ag phase, showing a perfect ordering in spite of a LT deposition of Ag adatoms. Such large domains of the $\sqrt{21}\times\sqrt{21}$-Ag structure produce the sharp LEED spots shown in Fig. 1(b). Figure 8 shows bias-dependent STM images of the $\sqrt{21}\times\sqrt{21}$-Ag phase, ranging from filled-state images [Figs. 8(a)–8(c)] to empty-state images [Figs. 8(d)–8(f)]. The images looks quite different depending on the bias voltage; a propellerlike pattern in one of the half-unit cell at filled-state images [Figs. 8(a)–8(c)] changes to a ring pattern at corners of the unit cell in the empty-state images [Figs. 8(d) and 8(e)], and finally to a triangular network pattern with much weaker contrast in Fig. 8(f). These indicate that the images reflect the electronic states mainly, rather than topography. It should be pointed out here that the Au-adatom-induced $\sqrt{21}\times\sqrt{21}$-(Ag+Au) structure exhibits quite similar images; the image of Ichimiya *et al.* looks like Fig. 8(d),[1] and that of Nogami *et al.* resembles Fig. 8(e).[2] By taking the energy-band diagram [Fig. 6(a)] into consideration, the filled-state images [Figs. 8(b) and 8(c)] with biasvoltages of less than 1 V should reflect the distribution of S_1^* band, while the Fig. 8(a), with a bias-voltage of 1.5 V, should include the contributions of D and S_2' bands. Therefore, the Fig. 8(a) shows more localized states, exhibiting a clear propellerlike pattern with sharp contract, while images of smaller bias-voltages like Figs. 8(c) and 8(d) show more extended states in which the protrusions are vague and connected each other.

IV. DISCUSSIONS

In recent first-principles calculations for a model system with a $\sqrt{3}\times\sqrt{3}$ superstructure, in which an Ag adatom per unit cell was adsorbed upon the Si(111)-$\sqrt{3}\times\sqrt{3}$-Ag surface for imitating the $\sqrt{21}\times\sqrt{21}$-Ag structure,[17] a dispersive surface-state band crossing E_F was predicted, which is quite similar to the S_1^* band observed here. In the calculation the S_1^*, if any, is assumed to be mostly derived from the S_1 state of the initial $\sqrt{3}\times\sqrt{3}$-Ag substrate, which seems to be plausible because of the similarity found here between the S_1^* and S_1 states about the dispersions and the $p_{x,y}$ components. Since the dispersion of the S_1^* band in Fig. 6(a) is nicely parabolic, $\epsilon = \hbar^2 k^2/2m^*$ (where ϵ and k are the energy and wave vector, respectively, and $\hbar$ is the Planck's constant divided by 2π), the effective mass m^* of electrons in this band can be estimated to be $m^* = (0.29 \pm 0.02) m_e$, where m_e is the free electron's rest mass. This value of m^* is the same as

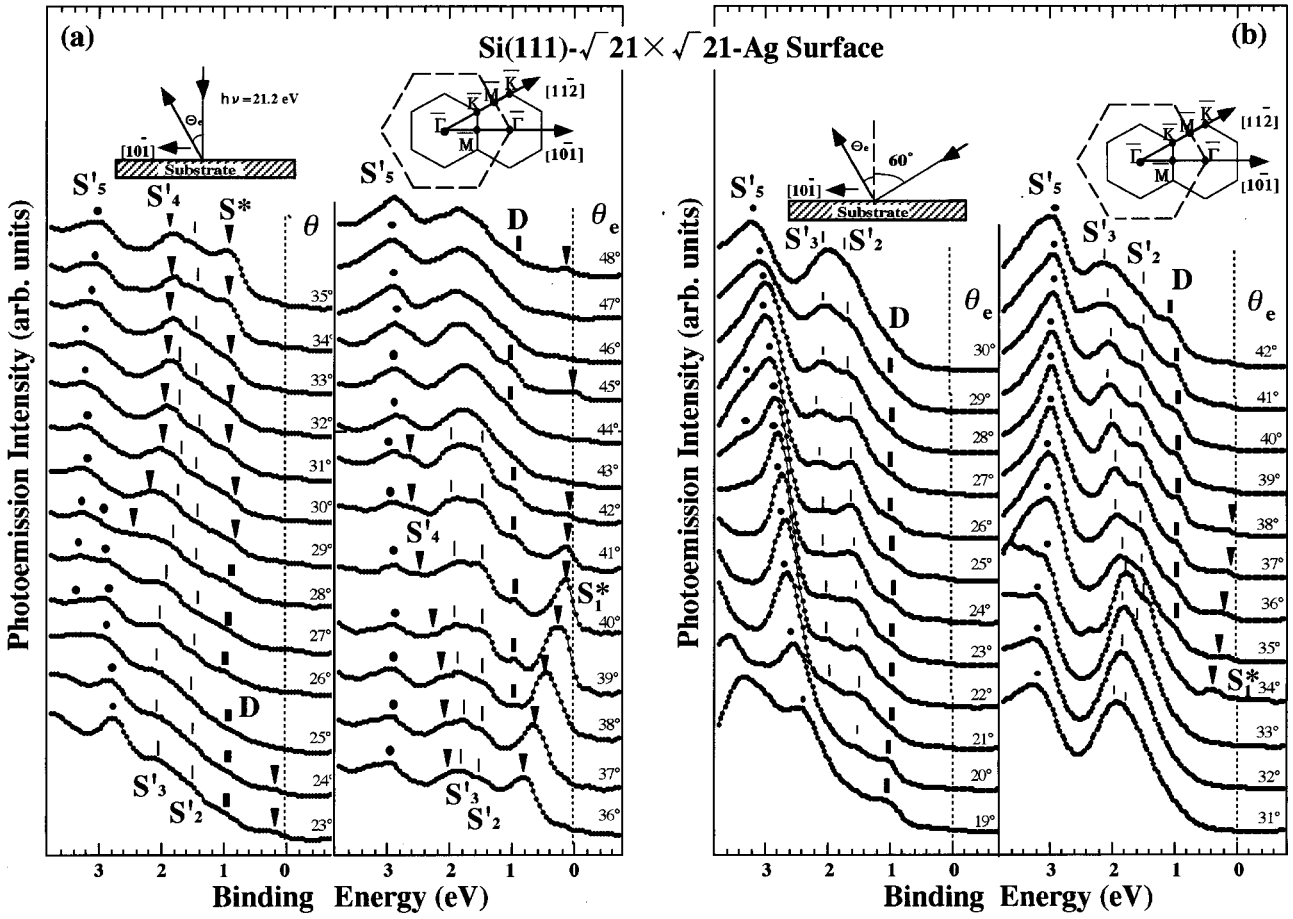

FIG. 5. ARPES spectra for the Si(111)-$\sqrt{21}\times\sqrt{21}$-Ag surface at 140 K taken with linearly polarized synchrotron radiation of 21.2 eV, scanned along the [10$\bar{1}$] direction. θ_i was (a) 0° and (b) 60°, respectively.

that in the S_1 band of the initial $\sqrt{3}\times\sqrt{3}$-Ag substrate found in a previous paper [$m^*=(0.29\pm0.05)m_e$],[19] and is comparable to that of conduction electrons in bulk silicon crystal $m^*=0.33m_e$. Then, the electron concentration trapped in the S_1^* band can be estimated by assuming the S_1^* band to be isotropic like the S_1 band. Since the density of states in a unit volume of a two-dimensional free-electron system is given by a constant $D=m^*/\pi\hbar^2$, the charge density $Q_{S_1^*}$, filled in

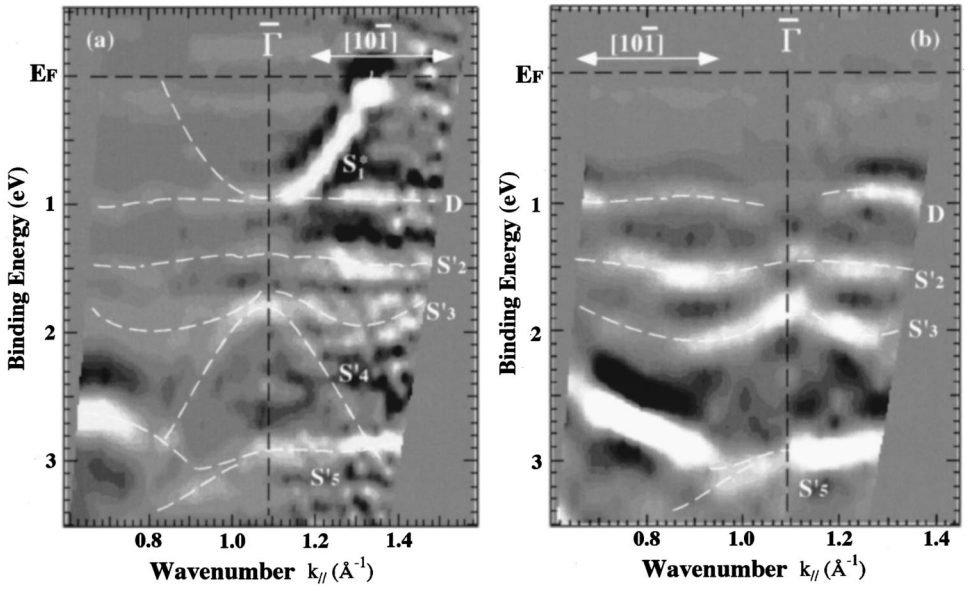

FIG. 6. Gray-scale band-dispersion diagrams for the Si(111)-$\sqrt{21}\times\sqrt{21}$-Ag surface, corresponding to the ARPES spectra in Figs. 5(a) and 5(b), respectively. The symbol $\bar{\Gamma}$ is the center of the second $\sqrt{3}\times\sqrt{3}$-surface Brillouin zone.

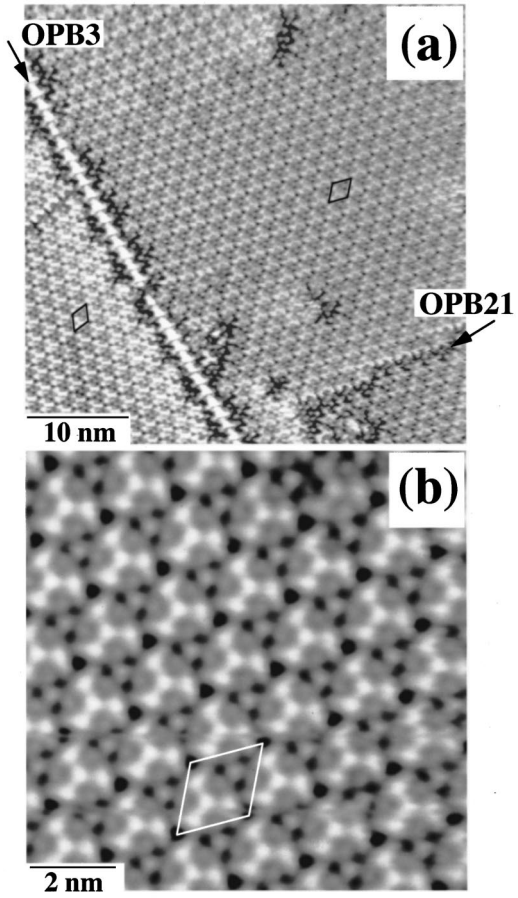

FIG. 7. Filled-state STM images of the Si(111)-$\sqrt{21}\times\sqrt{21}$-Ag surface taken at 70 K with a tip-bias voltage of 1.5 V and a tunneling current of 0.5 nA; (a) 43.5×43.5 nm^2 in the constant-height mode, and (b) its magnified image, 11×11 nm^2 in the constant-current mode. The $\sqrt{21}\times\sqrt{21}$ unit cells are drawn.

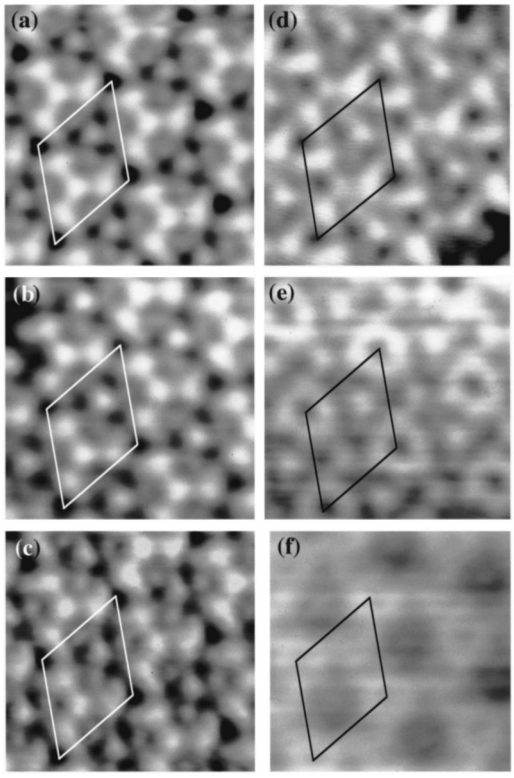

FIG. 8. A series of bias-dependent STM images of the Si(111)-$\sqrt{21}\times\sqrt{21}$-Ag surface taken at 70 K. Filled-state images (a) with a tip-bias voltage $V_T=1.5$ V and tunneling current $I_T=0.5$ nA; (b) $V_T=1.0$ V and $I_T=1.2$ nA, (c) $V_T=0.5$ V and $I_T=0.35$ nA. Empty-state images: (d) $V_T=-0.5$ V and $I_T=0.4$ nA; (e) $V_T=-1.0$ V and $I_T=0.9$ nA; (f) $V_T=-1.5$ V and $I_T=1.0$ nA. A $\sqrt{21}\times\sqrt{21}$ unit cell is drawn in each image.

the S_1^* band, is $Q_{S_1^*}=-D\epsilon=-1.2\times10^{14}e/\mathrm{cm}^2$, where e is the elementary charge and ϵ is the bottom energy of the band with respect to E_F (0.95 eV). The electron concentration trapped in the S_1 band of the initial $\sqrt{3}\times\sqrt{3}$-Ag surface is obtained in the same way to be $Q_{S_1}=-1.8\times10^{13}e/\mathrm{cm}^2$. Therefore, the increase of the electron concentration in the surface-state bands is given by $\Delta Q_{S1*}=-1.0\times10^{14}e/\mathrm{cm}^2$, which is the origin of the very high electrical conductance of the $\sqrt{21}\times\sqrt{21}$-Ag surface;[8] from the core-level photoemission spectroscopy (PES) measurements which will be reported elsewhere,[20] the surface-space-charge-layer conductivity play no role in the high surface conductivity for the $\sqrt{21}\times\sqrt{21}$-Ag phase. The electrons in the S_1^* band are donated by Ag adatoms, which was evidenced by Si $2p$ core-level PES measurements that showed that accumulated holes in the surface space-charge layer under the initial $\sqrt{3}\times\sqrt{3}$-Ag surface are depleted under the $\sqrt{21}\times\sqrt{21}$-Ag surface,[20] meaning that the substrate also accepts some electrons from the Ag adatoms. This charge transfer is quite similar to the cases of Au- and Cu-induced $\sqrt{21}\times\sqrt{21}$-Ag superstructures.[9,10] This picture of electron donation from the adatoms was also supported by a theoretical calculation.[17]

Since the valence electrons of Ag adatoms are $5s$-orbital electrons, the $p_{x,y}$ character of the S_1^* state implies that the valence electron of the Ag adatom is completely transferred and injected into the S_1^* band of the $\sqrt{21}\times\sqrt{21}$-Ag phase to be delocalized, rather than localized when framing ionic covalent bonds between the Ag adatoms and the substrate. We should compare the present results for the $\sqrt{21}\times\sqrt{21}$-Ag surface with those in the Au-adatom-induced $\sqrt{21}\times\sqrt{21}$-(Ag+Au) phase found in a previous paper.[9] An S_1^* band with a similar dispersion also appeared at the $\sqrt{21}\times\sqrt{21}$-(Ag+Au) surface. However, another dispersive metallic band noted S_1', that also crossed E_F with a shallower bottom below E_F, was observed in the $\sqrt{21}\times\sqrt{21}$-(Ag+Au) surface. It was assigned theoretical calculations to be an adatom-induced band.[17] However, this band is not observed in the $\sqrt{21}\times\sqrt{21}$-Ag surface in the present study. Here we can guess that the S_1' band is located above E_F for the $\sqrt{21}\times\sqrt{21}$-Ag surface, so that it is not detected by PES, because the atomic structures should be similar to each other between Au- and Ag-adatom-induced $\sqrt{21}\times\sqrt{21}$ phases;[6] thus the electronic states also should be similar to each other, as suggested by their newly identical STM images. The calculation shows that the S_1' band is located very close to E_F,[17] so that it can be empty on the real surface. Since the other bands lie

in the deeper region, the S_2', S_3', S_4', and S_5' bands observed on the $\sqrt{21}\times\sqrt{21}$-Ag surface closely resemble the S_2, S_3, S_4, and S_5 bands, respectively, on the initial $\sqrt{3}\times\sqrt{3}$-Ag surface in the intensity distribution, dispersion, and symmetry. Therefore, it is quite plausible to suggest that they are equivalent bands, reflecting their similar substrate reconstructions. This supports a suggestion contained in all of the proposed atomic models of $\sqrt{21}\times\sqrt{21}$ phases, in which the $\sqrt{3}\times\sqrt{3}$ structure under the Ag(Au) adatoms are preserved.[2,1,21] The energy positions of these bands shift away from E_F about 0.4 eV compared to the corresponding bands in the $\sqrt{3}\times\sqrt{3}$-Ag surface. This is because a downward band bending occurs during a surface-structure conversion from the $\sqrt{3}\times\sqrt{3}$-Ag into $\sqrt{21}\times\sqrt{21}$-Ag structure, as also shown in Si $2p$ core-level PES.[20] The initial $\sqrt{3}\times\sqrt{3}$ surface is negatively charged due to electron transfer from the bulk to the S_1 surface-state band, while the $\sqrt{21}\times\sqrt{21}$-Ag surface become neutral due to electron transfer from Ag adatoms to the bulk state (and also to the surface state S_1^*). In other words, the surface space-charge layer under the initial $\sqrt{3}\times\sqrt{3}$-Ag structure is a hole-accumulation layer, while that under the $\sqrt{21}\times\sqrt{21}$-Ag surface is a depletion layer. Therefore, the electrical conductivity through the surface space-charge layer is reduced by the structure conversion. However, the measured conductance is greatly enhanced.[8] This is due to the surface-state band S_1^*, as mentioned above. An additional, rather dispersionless band, indicated by D at a binding energy around 1.0 eV that is detected only for the $\sqrt{21}\times\sqrt{21}$-Ag surface, would be an intrinsic band of the $\sqrt{21}\times\sqrt{21}$-Ag structure, because such a band was not recognized for the initial $\sqrt{3}\times\sqrt{3}$-Ag substrate. Since Ag adatoms are bonded to the $\sqrt{3}\times\sqrt{3}$-Ag substrate just by electron transfer without orbital hybridizations, as discussed above and also in a previous paper,[9] it is very unlikely that the D band is a bonding state between the Ag adatom and the $\sqrt{3}\times\sqrt{3}$-Ag substrate; rather, it may be a bonding state among the Ag adatoms. In all the atomic models for $\sqrt{21}\times\sqrt{21}$ structures,[1,2,21] the nearest-neighbor distance between the adatoms is 3.84 Å, which is much larger than that in bulk Ag crystal (2.89 Å) (with a face-centered-cubic structure). Therefore, the flatness of the D band can be interpreted by a small overlap integral between the neighboring adatom orbitals, due to the large separation among them. It is interesting to compare the S_4' (S_4) band with the S_1^* (S_1) band; both bands consist mainly of p_x and p_y components, and appear in similar parabolic dispersions, but in opposite ways (upward or downward). Therefore, it is reasonable to suggest that S_1^* (S_1) and S_4' (S_4) are a pair of bands in some relation, though the details are an open question. Since these are observed in both $\sqrt{3}\times\sqrt{3}$-Ag and $\sqrt{21}\times\sqrt{21}$-Ag surfaces, they should be related to the $\sqrt{3}\times\sqrt{3}$-Ag substrate. The calculations do not provide any interpretation for this point.[22,17,23]

V. CONCLUSIONS

Polarization-dependent ARPES was used to analyze the electronic band structure of Si(111)-$\sqrt{3}\times\sqrt{3}$-Ag and Si(111)-$\sqrt{21}\times\sqrt{21}(R\pm 10.89°)$-Ag surfaces at l40 K. The S_1 and S_4 bands consist mainly of p_x and p_y components with no measurable polarization dependence, while the S_3 state has an even symmetry with respect to a plane defined by the surface-normal and [101] directions, consisting primarily of p_z components. The S_2 and S_5 states have an s-orbital character. The S_1 band is detected in the $\bar{\Gamma}$-$\bar{K}$ direction as well as the $\bar{\Gamma}$-$\bar{M}$ direction, and has similar dispersions in both directions, which agrees well with theoretical calculations and suggests an approximately isotropic 2D nearly-free-electron-like state. The surface-state bands S_1–S_5 on the $\sqrt{3}\times\sqrt{3}$-Ag surface were found to remain in the $\sqrt{21}\times\sqrt{21}$-Ag structure, denoted as S_1^*–S_5', respectively. This supports a suggestion in all the proposed atomic arrangement models of the $\sqrt{21}\times\sqrt{21}$ structures, that the adatoms sit on a basically unaltered $\sqrt{3}\times\sqrt{3}$-Ag surface, and also suggests there is no covalentlike bonding between the adatom and the substrate. However, compared with the surface-state bands of the initial $\sqrt{3}\times\sqrt{3}$-Ag surface, those of the $\sqrt{21}\times\sqrt{21}$-Ag structure are shifted in energy position toward higher binding energy. This is due to electron transfer from the Ag adatoms into the S_1^* surface-state band and also into the bulk state (causing a downward band bending). An additional intrinsic flat band D was found on the $\sqrt{21}\times\sqrt{21}$-Ag surface at a binding energy of about 1.0 eV, and was tentatively assigned to be a bonding state among the Ag adatoms. The adatoms chemically bond with each other, but loosely bond with the $\sqrt{3}\times\sqrt{3}$-Ag substrate via charge transfer into the extended surface state S_1 of the substrate.

ACKNOWLEDGMENTS

This work was supported in part by Grants-In-Aid from the Ministry of Education, Science, Culture, and Sports of Japan, especially through the Creative Basic Research Program (No. 08NP1201) conducted by Professor Katsumichi Yagi of Tokyo Institute of Technology. We were also supported by CREST (Core Research for Evolutional Science and Technology) of the Japan Science and Technology Corporation (JST), conducted by Professor Masakazu Aono of Osaka University and RIKEN, and by the Special Researcher of Basic Science Program in RIKEN.

*Email address: tong@postman.riken.go.jp

[1] A. Ichimiya, H. Nomura, Y. Horio, T. Sato, T. Sueyoshi, and M. Iwatsuki, Surf. Rev. Lett. **1**, 1 (1994) (Au-adatom-induced $\sqrt{21}\times\sqrt{21}$ at RT).

[2] J. Nogami, K.J. Wan, and X.F. Lin, Surf. Sci. **306**, 81 (1994) (Au-adatom-induced $\sqrt{21}\times\sqrt{21}$ at RT).

[3] I. Homma, Y. Tanishiro, and K. Yagi, in *The Structure of Surfaces 3*, edited by S.Y. Tong, M.A. Van Hove, K. Takayanagi, and X.D. Xie (Springer, Berlin, 1991), p. 610 (Cu-adatom-induced $\sqrt{21}\times\sqrt{21}$ at RT).

[4] Z.H. Zhang, S. Hasegawa, and S. Ino, Phys. Rev. B **52**, 10 760 (1995) (Ag-adatom-induced $\sqrt{21}\times\sqrt{21}$ at LT).
[5] S. Hasegawa, K. Tsuchie, K. Toriyama, X. Tong, and T. Nagao, Appl. Surf. Sci. **39**, 3815 (2000) (alkali-metal-adatom-induced $\sqrt{21}\times\sqrt{21}$ at RT).
[6] M. Lijadi, H. Iwashige, and A. Ichimiya, Surf. Sci. **357/358**, 51 (1996) (Au- and Ag-adatom-induced $\sqrt{21}\times\sqrt{21}$ at RT and LT).
[7] C.-S. Jiang, X. Tong, S. Hasegawa, and S. Ino, Surf. Sci. **376**, 69 (1997) (Au-adatom-induced $\sqrt{21}\times\sqrt{21}$ at RT).
[8] X. Tong, S. Hasegawa, and S. Ino, Phys. Rev. B **55**, 1310 (1997) (Ag-adatom-induced $\sqrt{21}\times\sqrt{21}$ at LT).
[9] X. Tong, C.-S. Jiang, and S. Hasegawa, Phys. Rev. B **57**, 9015 (1998) (Au-adatom-induced $\sqrt{21}\times\sqrt{21}$ at RT).
[10] X. Tong, C.-S. Jiang, K. Horikoshi, and S. Hasegawa, Surf. Sci. **449**, 125 (2000) (Au- and Cu-adatom-induced $\sqrt{21}\times\sqrt{21}$ at RT).
[11] I. Matsuda, H.W. Yeom, K. Tono, and T. Ohta, Phys. Rev. B **59**, 15 784 (1999).
[12] X. Chen, H.W. Yeom, T. Abukawa, Y. Takauwa, Y. Mori, T. Shimatani, A. Kakizaki, and S. Kono, J. Electron Spectrosc. Relat. Phenom. **80**, 147 (1996).
[13] H.W. Yeom, T. Abukawa, Y. Takakuwa, M. Nakamura, M. Kimura, A. Kakizaki, and S. Kono, Phys. Rev. B **53**, 1948 (1996).
[14] T. Takahashi and S. Nakatani, Surf. Sci. **283**, 17 (1993), and references therein; T. Takahashi, S. Nakatani, N. Okamoto, T. Ishikawa, and S. Kikuta, Jpn. J. Appl. Phys. **27**, L753 (1988); Surf. Sci. **242**, 54 (1991).
[15] M. Katayama, R.S. Williams, M. Kato, E. Nomura, and M. Aono, Phys. Rev. Lett. **66**, 2762 (1991).
[16] L.S.O. Johansson, E. Landemark, C.J. Karlsson, and R.I.G. Uhrberg, Phys. Rev. Lett. **63**, 2092 (1989); **69**, 2451 (1992).
[17] H. Aizawa and M. Tsukada, Phys. Rev. B **59**, 10 923 (1999).
[18] Y.G. Ding, C.T. Chan, and K.M. Ho, Phys. Rev. Lett. **67**, 1454 (1991); **69**, 2452 (1992).
[19] Y. Nakajima, S. Takeda, T. Nagao, and S. Hasegawa, Phys. Rev. B **56**, 6782 (1997).
[20] X. Tong, S. Ohuchi, T. Sekigucghi, T. Tanikawa, K. Horikoshi, T. Nagao, A. Harasawa, T. Okuda, T. Kinoshita, and S. Hasegawa, Appl. Surf. Sci. (to be published).
[21] X. Tong, Y. Sugiura, T. Nagao, T. Takami, S. Takeda, S. Ino, and S. Hasegawa, Surf. Sci. **408**, 146 (1998) (Ag-adatom-induced $\sqrt{21}\times\sqrt{21}$ at RT).
[22] H. Aizawa, M. Tsukada, N. Sato, and S. Hasegawa, Surf. Sci. **429**, L509 (1999).
[23] S. Watanabe, M. Aono, and M. Tsukada, Phys. Rev. B **44**, 8330 (1991); Surf. Sci. **287/288**, 1036 (1993).